

# Air-supported Biaxial Bulge Tests on Structural Sealant Silicones and Polyurethane

Tom Reisewitz, Moritz Hajduk, Geralt Siebert

University of the Bundeswehr Munich, Germany, [Tom.Reisewitz@unibw.de](mailto:Tom.Reisewitz@unibw.de)

## Abstract

Structural glazing joints in glass structures are subject to dynamic seismic loads in certain regions. However, to date, there is no accepted proposal for the design of such situations. The seismic design of glass structures is either neglected or performed with equivalent values for the whole building. Not considering the behavior of the bonded joints under dynamic loading might be insufficient, especially in the presence of heavy glass elements. A more thorough investigation of the structural performance of silicone or polyurethane within bonded glass structures under different loading scenarios is urgently required and an appropriate material model is essential. The calibration of such a model is crucial to better understand the performance under dynamic loading. However, structural glazing joints are subjected to different combinations of stress states, especially under dynamic seismic loading, which are difficult to model using only uniaxial tests. For this purpose, air-supported bulge tests are performed on two different silicones and a polyurethane to analyze the material behavior under biaxial stress conditions. The tests are performed using air pressure instead of a liquid that causes the material to bulge until failure. Digital image correlation is used to measure deformation and, together with the internal pressure, to calculate the resulting stresses and strains across the surface. A circular opening in the testing machine, into which the test specimens are clamped and inflated, results in an almost perfect section of a spherical surface. Using Barlow's formula together with the recorded deformation and the measured internal pressure, the biaxial stress can then be calculated. These experiments are therefore critical to the calibration of an appropriate material model.

## Keywords

SSG, adhesive, bulge test, facade, silicone, polyurethane

## Article Information

- Published by [Glass Performance Days](#), on behalf of the author(s)
- Published as part of the Glass Performance Days Conference Proceedings, June 2025
- Editors: Jan Belis, Christian Louter & Marko Mökkönen
- This work is licensed under a [Creative Commons Attribution 4.0 International](#) (CC BY 4.0) license.
- Copyright © 2025 with the author(s)

## 1. Motivation and Introduction

Structural silicone glazing rarely experiences purely uniaxial tensile or compressive loads in practical applications. Under extreme loading conditions, such as seismic impacts, silicone joints undergo significant deformations and complex biaxial stress states, causing their material behavior to deviate significantly from that observed under uniaxial loading. However, their mechanical properties under these conditions have not yet been fully investigated. Drass (2020) has already conducted bulge tests on structural silicone adhesive. Circular specimens with a thickness of approximately 1 mm and an inner clamping ring diameter of 40 mm were tested to ensure that deformations remained within the measurement range of the optical system. The experiments were performed using water pressure, documenting failure pressures and the pressure-strain curve. However, no stress values were determined. His work builds on previous research on elastomers, particularly by Sasso et al. (2008), who combined bulge, uniaxial, and planar tensile tests to calibrate numerical material models. Their tests were conducted on small specimens using hydraulic pressure. Machado et al. (2012) further advanced bulge test analysis by integrating the 3D-DIC technique, enabling the independent determination of stress-strain fields without assumptions regarding axial symmetry. Their experiments were conducted on specimens with a diameter of 90 mm and a thickness of 2 mm using air pressure. There are several other studies that will not be discussed further here. The objective of this study is not to define detailed stress-strain curves for individual specimens. Instead, the aim is to determine average values from several samples and compare the properties of two silicones approved for SSG applications under biaxial stress with those of polyurethane. These results, along with additional experiments and stress states, will be incorporated into the calibration of a numerical material model to achieve a more comprehensive characterization of polymer behavior under different stress conditions.

## 2. Methods

Before presenting the tests and the test results, the mechanical principles for evaluating the tests are explained in more detail. An overview of the design and function of the test equipment and the manufacture of the test specimens is also provided.

### 2.1. Barlow's formula

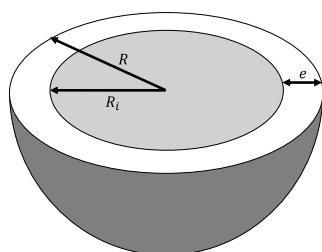


Figure 1: Cross-sectional area.

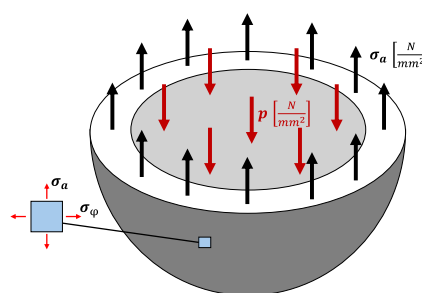


Figure 2: Cross-sectional area with loads.

Barlow's formula, which applies to thin-walled spherical or cylindrical pressure vessels, can be used to determine the equibiaxial stresses that arise in a bulge test, provided that the wall thickness is significantly smaller than the radius ( $e \ll R$ ). When a specimen in the bulge test is exposed to internal pressure  $p$ , it expands into a spherical shape, causing axial and tangential stresses to develop within the vessel wall (see [Figure 1](#) and [Figure 2](#)). Due to the assumption that  $e \ll R$ , radial stress can be neglected. Since the internal pressure  $p$  is exerted uniformly in all directions, it acts on the entire cross-sectional area:

$$A = \pi * R_i^2 \quad (1)$$

with a force of:

$$F_p = p * \pi * R_i^2 \quad (2)$$

Considering an arbitrary cross-section through the sphere's center, the axial stress  $\sigma_a$  and the tangential stress  $\sigma_\varphi$  can be determined. Given the thin-walled condition ( $e \ll R$ ),  $\sigma_a$  can be assumed to remain constant throughout the entire thickness of the shell. This leads to a force equilibrium expressed as:

$$\sigma_a * 2 * \pi * R_i * e - p * \pi * R_i^2 = 0 \quad (3)$$

Solving for  $\sigma_a$  yields:

$$\sigma_a = \frac{p * R_i}{2 * e} \quad (4)$$

This is called Barlow's formula. Since the sphere is perfectly symmetric, axial and tangential stresses  $\sigma_a$  and  $\sigma_\varphi$  are equal at every point on the shell and in all directions. For an infinitesimally small surface element, the curvature can be neglected, and the corresponding stress tensor in Cartesian coordinates is given by:

$$\sigma_{ij} = \begin{bmatrix} \sigma_{xx} & 0 & 0 \\ 0 & \sigma_{yy} & 0 \\ 0 & 0 & 0 \end{bmatrix} \quad (5)$$

Where:

$$\sigma_{ij} = \sigma_{xx} = \sigma_{yy} \quad (6)$$

This is classified as an equibiaxial stress state because both principal stresses are identical. For materials that experience considerable volume expansion under internal pressure, the conventional derivation of Barlow's formula becomes insufficient. The assumption that the wall thickness  $e$  remains constant is no longer valid, as it changes with volume expansion. Additionally, the classical Barlow's formula estimates stress based on a simplified annular cross-sectional area of:

$$2 * R_i * \pi * e \quad (7)$$

which is derived by unrolling the inner circumference and multiplying it by the wall thickness. However, a more accurate formulation requires considering the difference between the outer and inner circular areas. This leads to the exact force equilibrium expression:

$$\sigma * (\pi * R^2 - \pi * R_i^2) = p * \pi * R_i^2 \quad (8)$$

By substituting:

$$R_i = (R - e) \quad (9)$$

and solving for  $\sigma$ , we obtain:

$$\sigma = \frac{p*(R-e)^2}{e*(2*R-e)} \quad (10)$$

We call this the modified Barlow's formula. The error that arises between the modified Barlow's formula according to equation 10 and the original Barlow's formula according to equation 4 is determined as:

$$\Delta Stress = \frac{p*(e-R)}{2*(2*R-e)} \quad (11)$$

If the outer surface strains of the shell are known and an incompressible material behavior is assumed, the current wall thickness  $e$  can be calculated using volume conservation and the deformation gradient. For the incompressible case, the following condition must be satisfied:

$$\det(\mathbf{F}) = 1 \quad (12)$$

The deformation gradient  $\mathbf{F}$  for the biaxial incompressible case therefore results from the following relationship:

$$\mathbf{F} = \mathbf{1} + Grad u \quad (13)$$

This results in:

$$\mathbf{F} = \begin{bmatrix} 1 + \varepsilon_x & 0 & 0 \\ 0 & 1 + \varepsilon_y & 0 \\ 0 & 0 & \frac{1}{(1+\varepsilon_x)(1+\varepsilon_y)} \end{bmatrix} = \begin{bmatrix} 1 + \varepsilon_x & 0 & 0 \\ 0 & 1 + \varepsilon_y & 0 \\ 0 & 0 & 1 + \varepsilon_z \end{bmatrix} \quad (14)$$

Using these equations, the strains in the z-direction can be solved as follows:

$$\varepsilon_z = \frac{1}{(1+\varepsilon_x)(1+\varepsilon_y)} - 1 \quad (15)$$

With the strains in the z-direction and the initial wall thickness  $e_0$ , the current wall thickness  $e_i$  can finally be determined as follows:

$$e_i = e_0 + e_0 * \varepsilon_z \quad (16)$$

Further information regarding Barlow's equation can be found in Gross et al. (2024).

## 2.2. Mullins effect

Elastomers exhibit various effects under mechanical loading that significantly influence their material behavior. One of the most well-known effects is the Mullins effect, which occurs particularly in filled elastomers (Mullins, 1969). This phenomenon describes the stiffness reduction caused by stress after the first loading cycle. The most significant decrease in the stress response occurs during this initial cycle, while in subsequent cycles, the effect gradually diminishes. The Mullins effect can be explained by various physical mechanisms, which will not be discussed in detail here. It is a complex phenomenon that is not yet fully understood. To make more precise predictions about material

behavior, a combination of phenomenological and macromolecular models will likely be necessary. Further information can be found in the review articles by Diani et al. (2009) and Denora and Marano (2024). In the context of this study, only the initial loading of the material was considered, which, however, has no impact on the failure points.

### 2.3. Specimen production

To prepare the specimens for this study, silicone sheets with a thickness of 2–3 mm were first produced using two different types of silicone (referred to as A and B in the following) and a polyurethane (PU). The process began by covering a glass pane with a polyethylene (PE) film. The adhesive was then applied centrally onto the PE film. Next, spacers were positioned at the corners of the PE film before placing a second glass pane, also covered with PE film, on top. The two glass panes were then pressed together and secured with clamps until the gap between them matched the thickness set by the spacers. This setup allowed the adhesive to spread evenly between the glass panes along with the PE film (see Figure 3). Due to the precisely defined layer thickness and the pressure exerted by the glass panes, a nearly uniform, circular adhesive sheet was formed. Once the adhesive had cured, the glass panes were removed, allowing the sheets to undergo further curing. To ensure precise specimen dimensions, a mechanical punching machine was used to cut circular specimens with a diameter of 205 mm for the bulge test, following pre-defined templates. Before conducting the tests, a speckle pattern was applied to the specimens to enable the detection of surface deformations using digital image correlation (DIC) (see Figure 4).

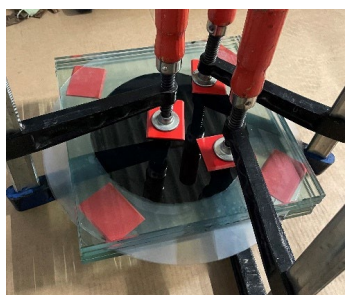


Figure 3: Specimen production.

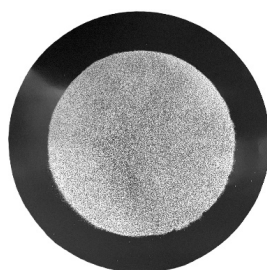


Figure 4: Specimen with pattern.

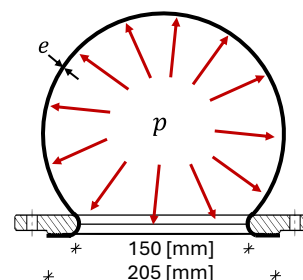


Figure 5: Pressure chamber.

### 2.4. Test device

The bulge test used in this study is a testing device designed to inflate circular membrane specimens, creating an equibiaxial stress state that can be increased up to failure if required. Unlike the procedure for sheet metal, specified in DIN EN ISO 16808 (2022), the specimens in this setup are not inflated using a liquid but rather with air pressure. Since there are no standardized guidelines for the bulge test on polymers, the following section provides a detailed explanation of the test apparatus and its functionality. The core component of the bulge test is the pressure chamber, which consists of a base plate and a clamping ring. Membrane specimens with a diameter of 205 mm can be clamped between these two components. The fixation is achieved using twelve M8 screws, which securely fasten the clamping ring to the base plate. The inner diameter of the clamping ring, where the specimen is inflated, measures 150 mm (see Figure 5).



Figure 6: Test stand with DIC.



Figure 7: Built-in specimen.

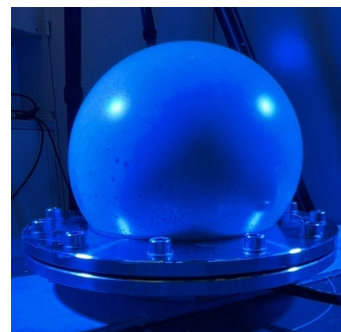


Figure 8: Specimen during test.

The inner edge of the clamping ring has a rounding radius of 6 mm to prevent mechanical damage to the specimen due to clamping. At the center of the base plate, there is a 20 mm opening through which compressed air is introduced to inflate the specimen. The pressure chamber is connected to a control unit and additional components via a compressed air hose and is designed for pressures of up to 10 bar. The pressure is recorded at a sampling rate of 20 Hz and output as an analog signal, which can be directly fed into the Digital Image Correlation (DIC) system. The test parameters can be adjusted flexibly, allowing for various loading scenarios, including biaxial tensile tests with variable pressure increase rates and creep tests with individually adjustable holding pressures and holding times or cyclic loads to investigate the Mullins effect under equibiaxial loads. However, it is not possible to generate negative pressures. The test stand setup is shown in Figure 6.

### 3. Experiments

Using the bulge test setup, equibiaxial tensile tests were performed on two silicones (referred to as A and B) and a PU. The PU is commonly used in railway vehicle construction for bonding glass panes and serves in this study as a comparison to the two structural silicones. All tests were conducted at approximately 20°C and recorded with DIC. The DIC system was initially started but only activated by a trigger signal (an analog signal) from the bulge test. This trigger signal was generated as soon as the test procedure in the bulge test commenced. After the tests were completed, a fitting sphere was adjusted to the surface of the inflated specimen based on the identified facet areas in the recorded images. This enabled the determination of the sphere's radius for each individual image. Simultaneously, the engineering strains in the two principal directions were calculated. In parallel, an analog signal from the bulge test directly transmitted the current internal pressure to the DIC system, ensuring that the pressure was known for each recorded image. Using the modified Barlow's formula (see equation 10), the stress at any given moment was then calculated. The actual wall thickness was determined based on the measured engineering strains in the two principal directions, assuming an incompressible material behavior. During these tests, the specimen membrane sealed the pressure chamber, where the internal pressure gradually increased at a ramp rate of 0.05 bar/s (0.005 MPa/s) until the specimen ultimately failed. A total of 25 specimens were tested: 12 from silicone A, 5 from silicone B and 8 from PU. Figure 7 illustrates the test specimen in its installed position prior to the start of the test. Figure 8 shows a test specimen during the experiment, where the characteristic spherical shape is distinctly visible. This validates the application of Barlow's formula for stress calculation. The image represents an example of one tested material. However, this shape was consistently observed across all tested materials, confirming the uniform deformation behavior under equibiaxial loading. The equibiaxial deformation could also be validated by the DIC measurement of the strains in the two main directions. Figure 9 and Figure 10: Error plot strains silicone. Figure 10 shows error plots of the strains, where almost no deviation can be seen.

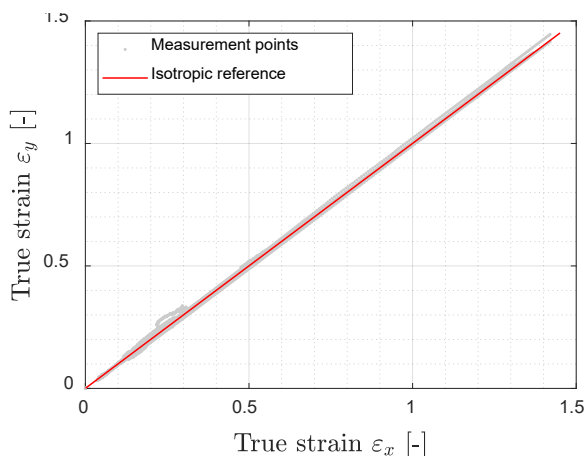


Figure 9: Error plot strains PU.

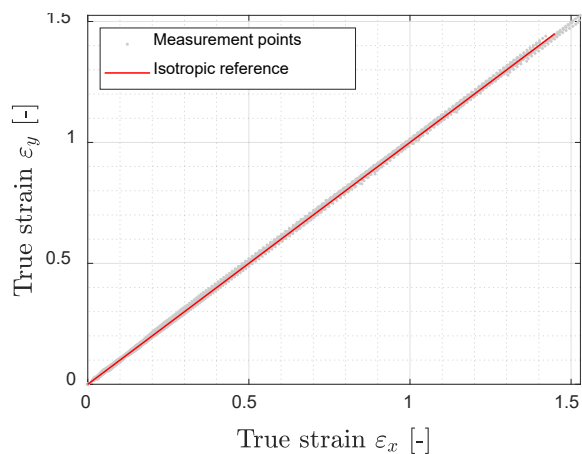


Figure 10: Error plot strains silicone.

### 3.1. Silicone A

Figure 11 presents the true stress over true strain curves obtained from the biaxial bulge tests conducted on Silicone A, including individual specimen responses as well as the corresponding mean stress-strain curve. The results indicate nonlinear material behavior, with an initial nearly linear elastic region, followed by a progressive increases. Compared to the other tested materials, Silicone A demonstrates a relatively low overall stress response for equivalent strain levels, indicating a more compliant mechanical behavior. The observed variations between individual specimens can be attributed to minor inconsistencies in material properties, specimen thickness, or experimental conditions such as the DIC measurement. However, the mean stress-strain curve provides a representative dataset suitable for material model calibration.

### 3.2. Silicone B

Silicone B, tested under identical conditions, exhibits a notably higher stress response across all strain levels (see Figure 12). This material follows a similar nonlinear trend, but its stiffness is significantly greater than that of Silicone A. The increased resistance to deformation suggests that Silicone B may be better suited for structural applications requiring higher load-bearing capacities. Despite minor variations among individual specimens, the mean curve offers a robust basis for numerical modeling. The observed differences between the two silicones emphasize the importance of material selection in applications where structural sealants must withstand biaxial tensile stresses, particularly in extreme loading scenarios. Further investigations into the fatigue and viscoelastic behavior of both materials under cyclic loading conditions are necessary to assess long-term performance.

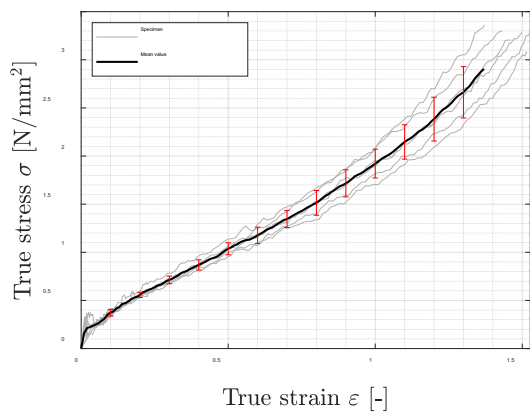


Figure 11: Silicone A.

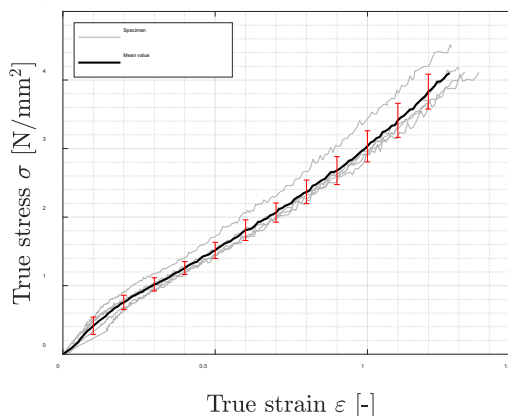


Figure 12: Silicone B.

### 3.3. Polyurethane

In contrast, the stress-strain curves obtained from the PU tests reveal a substantially higher stress response at comparable strain levels (Figure 13). The PU material demonstrates a pronounced strain-hardening effect, with true stress values significantly exceeding those of both silicone materials. This indicates a much stiffer mechanical behavior, making PU more resistant to deformation under equibiaxial tensile stress. The distinct stress-strain characteristics highlight the fundamental mechanical differences between PU and structural silicones. These results underline the necessity of tailoring material models specifically to each material class to ensure accurate predictions in structural applications.

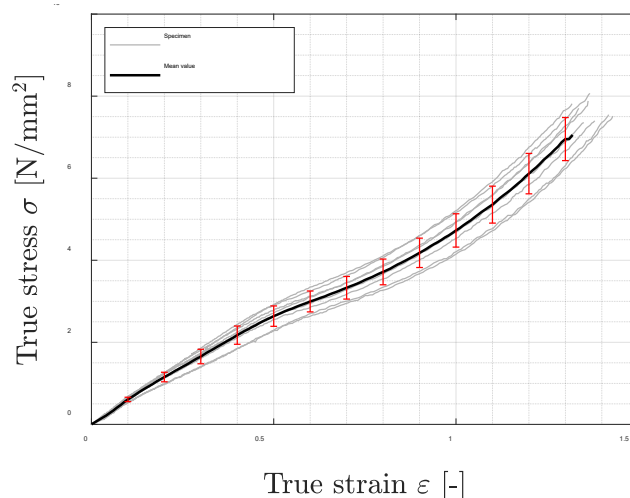


Figure 13: Polyurethane.

### 3.4. Failure behavior

The failure behavior of the tested materials, Silicone A, Silicone B, and PU was analyzed based on their respective true stress-true strain values at rupture. The results provide further insight into the mechanical differences between these materials under biaxial tensile stress and their potential applications in structural bonding. The failure points of Silicone A and Silicone B (Figure 14) exhibit distinct characteristics. Silicone A generally fails at lower stress levels but higher strain values. This suggests that Silicone A can withstand greater deformation before rupture but is limited in its ability to sustain high loads. In contrast, Silicone B reaches higher stress values before failure but at lower strain levels, demonstrating stiffer and stronger mechanical behavior. This means that Silicone B is better suited for applications requiring greater load-bearing capacity, while Silicone A offers enhanced flexibility. The differences in failure behavior between the two silicones confirm their distinct mechanical properties observed in the stress-strain curves, reinforcing the importance of material selection based on specific structural requirements. The PU specimens (Figure 15) show a significantly different failure response compared to the silicones. The true stress at failure exceeds 7.3 N/mm<sup>2</sup>, which is considerably higher than the failure stresses of both Silicone A and B, confirming the high load-bearing capacity of PU. In terms of strain, PU fails at values between 1.3 and 1.45, which is higher than Silicone B but lower than Silicone A. This indicates that PU, while not as flexible as Silicone A, still allows for a moderate degree of deformation before rupture. The combination of high strength and moderate deformation makes PU particularly suitable for applications that require high mechanical resistance, such as the bonding of glass panes in rail vehicle construction, where both high rigidity and a long service life are crucial. Overall, the comparison of the failure points between the silicones and PU confirms the results of the stress-strain analysis. PU is the strongest and stiffest material, able to withstand higher loads before failure, but it does not deform as much as silicone A. Silicone B offers intermediate mechanical behavior with a balance between strength and flexibility, while silicone A is the most compliant and ductile material, allowing for greater deformation before failure. These results are crucial for optimizing material selection in structural adhesive applications, as they ensure that the chosen material meets the specific mechanical requirements of the intended application. Typical failure patterns of silicones and polyurethane are shown in Figure 16 and Figure 17. The failure pattern of the silicones is characterized by a few cracks across the specimen, with no individual fragments. In the case of PU, on the other hand, there are many jagged cracks and several small fragments that detach completely from the test specimen.

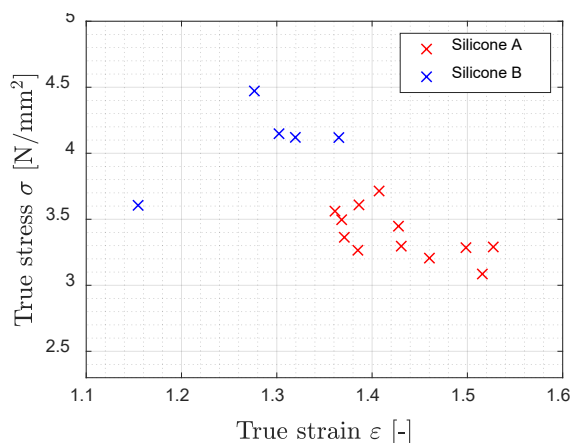


Figure 13: Failure points Silicone A and B.

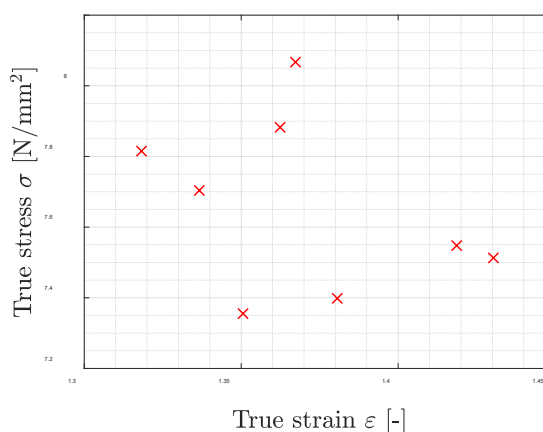


Figure 14: Failure points polyurethane.



Figure 15: Failure pattern silicone.



Figure 16: Failure pattern polyurethane.

#### 4. Conclusion and Outlook

The results of the biaxial bulge tests provide valuable insights into the mechanical behavior of the tested materials under equibiaxial tensile stress. The comparison of their stress-strain responses highlights significant differences in stiffness, strain-hardening behavior, and overall mechanical performance. Silicone A exhibited the most compliant behavior, with a lower stress response at equivalent strains, while Silicone B demonstrated higher stiffness and resistance to deformation, making it more suitable for applications requiring greater load-bearing capacity. In contrast, PU showed the highest stress values among all tested materials, indicating a much stiffer mechanical response, which aligns with its application in railway vehicle construction for glass bonding. These findings emphasize the importance of selecting appropriate materials based on their mechanical characteristics and intended application. The differences in stress-strain behavior between silicones and PU indicate that different modeling approaches are required to accurately predict their mechanical performance under real-world loading conditions. Structural silicones and polyurethanes, which are highly nonlinear, require advanced hyperelastic material models to correctly capture the deformation behavior.

In order to create a comprehensive and reliable material model, several important aspects need to be considered in future studies. First, additional biaxial tests under different loading conditions, including cyclic and dynamic loading, are required to capture viscoelastic effects and fatigue behavior. Furthermore, time-dependent material properties such as stress relaxation and creep behavior should be analyzed to improve the prediction accuracy of numerical simulations. A suitable material model for structural silicones should include hyperelastic formulations such as the Mooney-Rivlin or Ogden model in combination with viscoelastic elements to account for time-dependent behavior. To validate these models, structural tests should be performed on bonded components to allow a direct comparison between experimental results and numerical predictions. By taking these aspects into account, the accuracy of prediction models for bonded structures can be significantly improved, increasing the reliability and safety of applications with structural sealants and adhesives in engineering and architecture.

## References

- Denora, I., & Marano, C. (2024). Stretch-induced softening in filled elastomers: A review on Mullins effect related anisotropy and thermally induced recovery. *Polymer Testing*, 133, 108399. <https://doi.org/10.1016/j.polymertesting.2024.108399>
- Diani, J., Fayolle, B., & Gilormini, P. (2009). A review on the Mullins effect. *European Polymer Journal*, 45(3), 601–612. <https://doi.org/10.1016/j.eurpolymj.2008.11.017>
- DIN Deutsches Institut für Normung. (2022). DIN EN ISO 16808:2022-08. DIN Media GmbH. <https://doi.org/10.31030/3365427>
- Drass, M. (2020). *Constitutive Modelling and Failure Prediction for Silicone Adhesives in Façade Design* (Vol. 55). Springer Fachmedien. <https://doi.org/10.1007/978-3-658-29255-3>
- Gross, D., Hauger, W., Schröder, J., & Wall, W. A. (2024). *Technische Mechanik 2: Elastostatik*. Springer. <https://doi.org/10.1007/978-3-662-68423-8>
- Machado, G., Favier, D., & Chagnon, G. (2012). Membrane Curvatures and Stress-strain Full Fields of Axisymmetric Bulge Tests from 3D-DIC Measurements. Theory and Validation on Virtual and Experimental results. *Experimental Mechanics*, 52(7), 865–880. <https://doi.org/10.1007/s11340-011-9571-3>
- Mullins, L. (1969). Softening of Rubber by Deformation. *Rubber Chemistry and Technology*, 42(1), 339–362. <https://doi.org/10.5254/1.3539210>
- Sasso, M., Palmieri, G., Chiappini, G., & Amodio, D. (2008). Characterization of hyperelastic rubber-like materials by biaxial and uniaxial stretching tests based on optical methods. *Polymer Testing*, 27(8), 995–1004. <https://doi.org/10.1016/j.polymertesting.2008.09.001>